

A new method of estimating the mass-to-light ratio of the Ursa Minor dwarf spheroidal galaxy

M. Ángeles Gómez-Flechoso¹

Geneva Observatory, Ch. des Maillettes 51, CH-1290 Sauverny, Switzerland

D. Martínez-Delgado

Instituto de Astrofísica de Canarias, E-38205 La Laguna, Tenerife, Canary Islands, Spain

ddelgado@ll.iac.es

ABSTRACT

Dwarf satellite galaxies undergo strong tidal forces produced by the main galaxy potential. These forces disturb the satellite, producing asymmetries in its stellar distribution, tidal tail formation, and modifications of the velocity dispersions profiles. Most of these features are observed in the Ursa Minor (UMi) dwarf spheroidal galaxy, which is one of the closest satellites of the Milky Way. These features show that UMi is been tidally disrupted and probably not in virial equilibrium. The high velocity dispersion of UMi could also be a reflection of this tidal disruption and not the signature of the large dark matter content that would be deduced if virial equilibrium is assumed. In order to avoid the uncertainty produced when virial equilibrium is assumed in systems in strong tidal fields, we present a new method of calculating the mass-to-luminosity ratio of disrupted dwarf galaxies. This method is based on numerical simulations and only takes into account the shape of the dwarf density profile and the tidal tail brightness, but does not depend on the kinematics of the dwarf. Applying this method to UMi, we obtain a mass-to-luminosity relation of 12, which is lower than the value obtained assuming virial equilibrium ($M/L = 60$). In addition, if UMi has a large dark-matter content, it will be impossible to reproduce a tidal tail as luminous as the one observed.

Subject headings: Galaxy: formation — Galaxy: structure — Galaxy:halo — (Galaxy:) — galaxies: individual (Ursa Minor)

¹Present address: Universidad Europea de Madrid, E-28670 Villaviciosa de Odón, Madrid, Spain

1. Introduction

The simplest galactic systems, the dwarf spheroidal galaxies (dSphs), reveal high velocity dispersions that imply the highest known mass-to-light ratios (M/L) (see Mateo 1998 for a review). These large velocity dispersions are commonly interpreted in terms of the galaxies being embedded in a massive dark-matter halo. Alternative explanations are these mass-to-light ratios may be inflated owing to tidal effects (Hodge & Michie 1969; Gómez-Flechoso, Fux, & Martinet 1999), or that these systems are actually long-lived tidal remnants oriented close to the line of sight (Kroupa 1997).

Ursa Minor (UMi) is one of the closest satellites of the Milky Way ($d = 69$ kpc; Carrera, Aparicio, & Martínez-Delgado 2002) and, of these, shows, together with Draco, the highest observed velocity dispersion ($M/L = 60$; Mateo 1998). The discovery of a tidal extension in UMi (Martínez-Delgado et al. 2001) indicates that this galaxy is at an advanced stage of complete tidal disruption (see also Palma et al. 2002). In addition, the presence of lumpiness and asymmetry in the stellar distribution of UMi along its major axis (Olszewski & Aaronson 1985; Irwin & Hatzidimitriou 1995; Kleyna et al. 1998; Martínez-Delgado et al. 2001) could be reminiscent of tidally disrupted satellites (Kroupa 1997). The overall shape of the outer contours appears to be clearly S-shaped (Palma et al 2002; Martínez-Delgado et al. 2002, submitted), as is expected for a tidally disrupted system (i.e., the globular cluster Pal 5; see Odenkirchen et al. 2001). These observational features suggest that UMi may not be in virial equilibrium, supporting the idea of a possible tidal origin for UMi’s observed high radial velocity dispersion. This fuels the debate about the validity of the methodology used to infer the high M/L in dSphs and therefore the presence of large quantities of dark matter in these galaxies.

In this paper, we introduce a new method of estimating the mass of satellite dSph galaxies that are subjected to tidal forces. This method does not involve assumptions about the internal dynamics of the satellite can and therefore be used for satellites that are out of virial equilibrium. Using this method, we have analyzed the case of UMi and obtained a new value for the M/L ratio of this galaxy.

2. OBSERVATIONS AND TIDAL TAIL FORMATION MODEL

Observations, data reduction, and photometry of the UMi dSph galaxy used in this paper are described in detail in Martínez-Delgado et al. (2001) and Carrera et al. (2002). This wide-field survey revealed the presence of stellar members of UMi beyond the previous measured tidal radius, indicating the existence of a tidal extension in this galaxy. This tidal

extension could be spread out well beyond the area covered in our survey ($R > 80'$), as suggested by the presence of a “break” to a shallower slope observed in its density profile (see figure 3 in Martínez-Delgado et al. 2001).

In this paper, UMi’s observed surface brightness profile is compared with a theoretical model of tidally disrupted dSph satellites. The tidal tail is assumed to be formed by the tidal forces of the Milky Way potential, which are important at the galactocentric distance of UMi. The tidal forces produce deformations in the satellite structure and the disruption of the dwarf. The limit of the bound material, that is, the tidal radius, is determined by the equilibrium between the satellite potential well and the Milky Way halo potential well. This equilibrium can also translate into a relation between the satellite average density, $\bar{\rho}_S(< r_t)$, and the local and averaged densities of the Milky Way halo, $\rho_H(R)$ and $\bar{\rho}_H(< R)$ respectively. Details of the tidal limit calculations are given in Gómez-Flechoso & Domínguez-Tenreiro (2001). The unbound material, that forms the tidal tail and is placed beyond the tidal radius, is diffused into the Milky Way halo. As explained in Johnston, Sigurdsson, & Hernquist (1999), the surface density of the tidal tail approximately follows a power-law profile in the regions close to the dwarf. Obviously, the exponent of this power law depends on the amount of extra-tidal material close to the dwarf and has a steeper density profile when the amount of stripped material is low and vice versa. This amount of stripped material correlates with the strength of the Milky Way tidal force and therefore varies along the orbit, since the satellite travels through regions with different tidal fields. If the amount of stripped material is large, the tidal tail will have an almost constant mass density region close to the satellite (one example of that is the UMi tidal extension) with a tidal tail mass density similar to the satellite mass density at the tidal radius. In this case, the tail mass density correlates with the Milky Way potential at the position of the dwarf, since the satellite mass density at the tidal radius is proportional to the Milky Way potential, as we have explained above. So, for a given halo potential, shape of the satellite density profile, and position of the satellite in the halo, the mass density of the tidal tail in the region close to the tidal radius is fixed independently of the satellite mass. In Figure 1a the projected mass density profiles of three evolved satellite models have been plotted. These satellites have different initial-mass models and have formed a tidal tail after a few orbits. As can be seen in this figure, the central-region of the projected mass density of the satellites differs by up to a factor ten when comparing the different models; however, the tail mass density is almost the same independently of the models. More details of these models are given in Section 3.

Using these results, if we know the halo potential field we can estimate the mass density of the satellite galaxy at the tidal radius and therefore the tidal tail mass density. Once the mass density profile of the satellite and its tail are estimated, the M/L ratio of the dwarf can be calculated by fixing this M/L ratio to reproduce the observed central luminous surface

brightness of the satellite. Given two satellites with different mass densities and with the same central luminous surface brightness, the highest mass density satellite will have a larger M/L ratio than the low mass density one. Following this relation, if the two satellites with the same central luminous surface brightness are placed at the same point in the main galaxy potential, as the mass density of the tidal tail is the same for both satellite, the tail surface brightness of the denser satellite will be fainter than that of the low mass density satellite (assuming that a tidal tail has the same M/L ratio as its satellite). In Fig. 1b, the three satellite models of Figure 1a have been plotted assuming that all of them have a central surface brightness of $26 \text{ mag arcsec}^{-2}$. As can be seen in this figure, the denser model needs to have a larger M/L ratio to reproduce the same central surface brightness as the other models, and consequently its tidal tail is fainter. Assuming the same central luminous surface brightness for the satellite models, the differences in the central mass density translate into differences in the tail surface brightness. Only one satellite model will be able to reproduce, at the same time, the central luminous surface brightness and the tail luminous surface brightness of an observed satellite dwarf galaxy at a given position in the halo. Using this method, we can estimate the M/L ratio of the dwarf independently of its internal kinematics.

3. CALIBRATION OF THE TIDAL TAIL MODEL

As has been explained in the previous section, the mass density of a satellite tidal tail is independent of the satellite mass (given the shape of the satellite density profile and its position in the orbit). Using the observed surface brightness profile of the satellite, we can select the model that fits the luminous surface brightness of the satellite + tail system, and therefore the mass of the best fit model is a good estimate of the mass of the observed satellite galaxy. Consequently, the M/L ratio of the satellite dwarf can be calculated. Before using this method to estimate the mass of the dwarf satellites, we have to calibrate the sensitivity of the method to small differences in satellite mass (in other words, to study whether satellite models with different masses can reproduce the same satellite + tail density profile or not), to differences in the shape of the main galaxy potential and to variations of the dwarf orbit. In this way, we will know the accuracy of the calculations.

3.1. Effects of satellite total mass on tidal tail formation

To analyze how the mass content of a satellite is related to the tidal tail surface brightness, we have selected three satellite models with a King–Michie profile with the same dimensionless central potential, $W_o = 4$, and the same core radius, $r_o = 0.3 \text{ kpc}$ (which

corresponds to a tidal radius $r_c = 2.1$ kpc), but different total mass. The three total masses are 0.4×10^7 , 1.6×10^7 , and $4 \times 10^7 M_\odot$. These satellites have been placed in an orbit similar to that of UMi (Schweitzer, Cudworth, & Majewski 1997). In these models, we have selected an analytical logarithmic potential to roughly reproduce the Milky Way potential.² The shape of this logarithmic potential is $\Phi_H = v^2 \log(R^2 + z^2/h^2 + a^2)$ where $v = 170$ km s⁻¹, $a = 19.9$ kpc and $h = 1.0$. For this potential, the apocenter and pericenter of the orbit of the models are approximately 80 and 20 kpc, respectively.

In Figure 1b, we have plotted the surface brightness of the three satellite models with different initial total masses. The initial masses of the models do not give information about their masses at the moment of the figure snapshot, since the satellites have undergone tidal disruption. In order to better compare the models, the masses inside 1 kpc of each model are also listed in the figure. The three models have been calibrated in luminosity to have the same central surface brightness ($\mu_{v,o} = 26$ mag arcsec⁻¹). The calibration can be translated in terms of different M/L ratios, as explained in Section 2. This figure shows that the three brightness profiles have the same slope in the central regions. However, the luminous surface brightness of the tidal tails are closely related to the mass content. The lowest-mass satellite, with $M/L = 3.5$, develops quite a luminous tidal tail. In fact, this satellite only survives a few orbits in the halo potential. In contrast, the highest-mass satellite forms a low brightness tidal tail ($\mu_{v,tail} \sim 33.5$ mag arcsec⁻¹) and has a larger tidal radius ($r_t \sim 1.5$ kpc). The tidal tail of this massive model ($M/L = 50$) will not be observationally detected, assuming a typical satellite central surface brightness. Finally, the model with a moderate M/L ratio ($M/L = 13$) develops a tidal tail that could be detected with the present observational resolution, as its tidal tail surface brightness is $\mu_{v,tail} \sim 32$ mag arcsec⁻¹. In the same figure, the observational data for the surface brightness of UMi are plotted (black dots) in order to compare the models properly.

Summarizing these results, the effect of satellite mass content on tidal tail formation is quite important, as a variation of a factor 10 in mass produces a variation of a factor of 15 in the M/L ratio, assuming the same central surface brightness.

²In this section we are only interested in analyzing the effects of the satellite mass content in the tidal tail formation and not in reproducing the details of the morphological evolution of UMi.

3.2. Effects of halo potential oblateness of the main galaxy on tidal tail formation

The tidal tail surface brightness of a satellite in a given orbit is related not only to its mass content but also with the shape of the potential of the main galaxy. For this reason, we have estimated the importance of the main galaxy oblateness in satellite disruption. We have modeled the halo of the primary galaxy using the logarithmic potential of the previous section with the same v and a parameters, but with three different oblateness values, $h = 1.0, 0.8$, and 0.6 (oblateness values smaller than 0.6 in the potential are unrealistic, since they cannot be reproduced with any mass distribution). The satellite model is a King–Michie model with initial total mass $M_{\text{ini}} = 2 \times 10^7 M_{\odot}$, core radius $r_o = 0.3$ kpc and dimensionless central potential $W_o = 4$. The satellite orbit has been fixed on the assumption that it has the energy needed to reproduce the present position and velocity of UMi.

Figure 1c shows the surface brightness of the satellite after a few orbits for the three halo potential models. The snapshots used in this plot represent a satellite with the same position and velocity as UMi. This figure shows that it is possible to reproduce the same satellite and tidal tail profiles using a different halo potential; however, the final satellite mass content varies. The formation of dense tidal tails is more efficient in oblate potentials (for orbits such as that of UMi); therefore, the satellite needs fewer orbits to develop an observable tidal tail. Therefore, for the same initial satellite model, the larger oblateness of the halo is, the higher satellite mass content is necessary to reproduce the same satellite+tail surface brightness profile and, consequently, the larger M/L will be.

It is remarkable that the effect of the halo potential shape on the determination of the mass–luminosity ratio is fainter than the effect of the initial satellite mass. It can be seen that there is only a factor of two in the M/L ratio for the whole range of realistic values of the potential oblateness (that is, h between 1.0 and 0.6). However, a variation of a factor of 10 in the satellite mass produces a variation of a factor of 15 in the M/L ratio. This means that the potential shape only introduces a small indeterminacy in the satellite mass calculation.

3.3. Effects of small variations in the satellite orbit on tidal tail formation

Variations in the satellite velocity within the observational errors produce differences in the dwarf orbit and, consequently, in its apocenter and pericenter. As the tidal stripping of satellites depends on the orbit (the smaller pericenter of the orbit, the larger the tidal stripping), small differences in the orbit can affect the tidal tail formation. In order to

calibrate this effect, we have placed the same satellite model in three different orbits. One of these fits UMi’s velocity and position at the end of the simulation, while the other two orbits differ by $\pm 10\%$ in velocity from the previous one. The satellite model corresponds to a King–Michie model with core radius $r_o = 0.3$ kpc, initial total mass $M_{\text{ini}} = 1.6 \times 10^7 M_\odot$, and dimensionless central potential $W_o = 4.0$. The halo potential of the main galaxy is the spherical logarithmic potential described in Section 3.1. In Figure 1d, the surface brightness profiles of the models are shown. These three profiles, corresponding to the three orbits, are quite similar, only small differences in the M/L ratio can be observed. The satellite in the highest-velocity orbit shows the largest M/L ratio and vice versa, however, the M/L ratio difference between models are of the same order as their difference in orbital velocity.

The error in the M/L ratio calculation due to the observational errors of the satellite velocity is of the same order of magnitude as these observational errors. For observational errors of 10–20%, the satellite mass content is more important in the M/L determination than the effects introduced by small variations in the satellite orbit.

4. THE M/L RATIO OF THE URSA MINOR dSph

UMi shows observational features that reveal the existence of large tidal forces. Therefore, the simplify virial equilibrium theorem assumption is not justified for measuring the M/L ratio, but we should include all the variables in a more generalized expression. Instead of doing this, we have introduced a new method of mass calculation that does not involve the kinematics of the dwarf. In this section, we have analyzed the M/L ratio of the UMi dSph using the method described in Sections 2 and 3.

The Milky Way halo density is one of the parameters that determines the tidal tail density. Therefore assuming a realistic value for it is very important. The halo density can be deduced from the shape of the Milky Way halo potential. Such a potential can be inferred from the dynamics of stars of the Milky Way and the orbits of the dwarf satellite galaxies. Observational data of the tidal stream of the Sagittarius dwarf galaxy are therefore very valuable. The shape of the Sagittarius orbit is traced with the tidal debris of this satellite in a strip 100° long (see Martínez-Delgado et al. 2002 for details). We have used these observational data to fix the parameters of the Milky Way model. This is a quite realistic three-component model (halo + disk + bulge) that is described in detail in Fux (1997). The parameters of the final numerical model that reproduce the Milky Way potential are described in Gómez-Flechoso et al. (1999). Other density distributions of the Milky Way can also reproduce a similar potential well, compatible with the Sagittarius orbit. It is important to remark that the physical quantity that determines the satellite orbits is the potential of

the main galaxy, not its density distribution, and that, therefore, density distributions of the Milky Way halo with different shape and oblateness could reproduce the same results if they had similar potential wells. However, we recall that small variations in the shape of the main galaxy potential do not significantly change the results of the M/L ratio of the analyzed satellite, as shown in Section 3.2.

The UMi satellite has been represented by an N -body model orbiting in this Milky Way potential. The orbit is consistent with the observational proper motion of UMi (Schweitzer et al. 1997). We assume a UMi model of one component given by a King–Michie model and therefore the observed luminosity profile must be reproduced by the model density profile. The parameters of the King–Michie model that reproduces more accurately the shape of the density profile of UMi and its tidal tail are a core radius $r_o = 0.3$ kpc and a dimensionless central potential $W_o = 4.0$. However, the total mass of the model is still a free parameter that we calculated reproducing the central brightness of the dwarf and the tidal tail brightness at the same time (as described previously). The best fit is obtained with a model of total initial mass $M_{\text{ini}} = 4 \times 10^7 M_\odot$. The surface brightness profile of the UMi model and its tidal tail after roughly seven orbits is plotted in Figure 2 (dashed line). The observational UMi profile has also been represented in the same Figure (dots). As can be seen, the model provides a good fit of the observational data. We have assumed a mass-to-luminosity ratio $M/L = 12$ to adjust the central surface brightness of the model to that observed. In this snapshot, the total mass in the inner kiloparsec of the model is $0.79 \times 10^7 M_\odot$.

The value of the M/L ratio obtained using this new method of mass calculations is different from the matter content derived from the virial theorem ($(M/L)_{\text{virial}} = 60$; Mateo 1998). However, this lower value is very consistent with the new mass-to-light ratio estimate obtained by Palma et al. (2002), who reduce the mass-to-light ratio to $M/L \sim 16$, using a new estimate of the UMi total luminosity (which is 2.7 times greater than the previous values) and considering the (possible) effects of anisotropic velocity dispersions (Hodge & Michie 1969).

The observed velocity dispersion obtained for UMi is 7.6 km s^{-1} (Armandroff, Olszewski, & Pryor 1995). In our UMi model, the velocity dispersion at the center is 4 km s^{-1} and presents a rising profile that reaches 8 km s^{-1} on the outskirts of the dwarf (Martínez-Delgado, Gómez-Flechoso, Alonso-García & Aparicio 2003, in preparation). However, the observed velocity dispersion includes the effects of the substructures of the main body of UMi, and that could increase the velocity dispersion. This substructure cannot be reproduced with a numerical model because we do not have sufficient resolution to form condensations inside UMi and, therefore, the velocity dispersion of the UMi models is not expected to fit that observed. On the other hand, if UMi is assumed to be in virial equilibrium, the mass-to-

luminosity ratio obtained from its observational velocity dispersion ($(M/L)_{\text{virial}} = 60$) will produce a very low surface brightness tidal tail, which could not be observationally detected (see Figure 1b). Furthermore, the signatures of tidal disruption observed in UMi (internal substructure and tidal extension) make doubtful the existence of simple virial equilibrium in the internal region of UMi. In these dynamical conditions, our method seems to be more reasonable for the satellite mass calculation. However, new models with a higher resolution reproducing the internal dynamics of the UMi dSph and new observations of the UMi velocity dispersion profile are needed in order to understand the dynamical state of the dwarf.

5. CONCLUSIONS

We have developed a new method of estimating the mass of satellite galaxies subjected to tidal forces. This method does not involve suppositions about the internal dynamics of the satellite and can therefore be used for satellites that are out of virial equilibrium.

The main results of this model are that massive and dense satellites form low brightness tidal tails (for a given satellite central surface brightness), and that low-density satellites undergo strong tidal forces that produce comparatively bright tidal tails. Once the satellite central surface brightness is known, the main parameters that determine the tail brightness in the region close to the satellite tidal radius are the density profile and the mass content of the bound part of the satellite.

The shape of the primary galaxy potential can introduce small uncertainties in the satellite mass estimates that are no larger than a factor of two over the whole physical range of oblateness. The larger the halo oblateness is, the denser the tidal tail that is formed. The observational errors of the satellite orbital velocity can also introduce an uncertainty in the M/L ratio calculation, but this uncertainty is no larger than the errors in the satellite velocity.

Obviously, the tidal tail brightness depends on the satellite’s position in its orbit, since tail mass density depends on the halo potential at the satellite’s position. As the satellite travels along its orbit, it goes through different density regions and produces variations in the tidal tail brightness. So it is very important to know the satellite’s position in its orbit in order to estimate its mass content using this method. A satellite tidal tail can be observed when the satellite is in a given region of its orbit, but it can be too faint to be detected in other regions of the orbit.

Finally, we have applied the new method for the mass calculations to UMi. The results shows $M/L \sim 12$, in order to reproduce its luminosity profile and tidal tail brightness. The

tidal disruption features observed in UMi suggest that this dwarf is not in virial equilibrium. The observational data of the velocity dispersion profile could confirm this if they show the same rising profile as that of the model.

REFERENCES

- Armandroff, T. E., Olszewski, E. W., & Pryor, C. 1995, *AJ*, 110, 2131
- Carrera, R., Aparicio, A., & Martínez-Delgado, D. 2002, *AJ*, 123, 3199
- Fux, R. 1997, *A&A*, 327, 983
- Gómez-Flechoso, M. A., Fux, R., & Martinet, L. 1999, *A&A*, 347, 77
- Gómez-Flechoso, M. A., & Domínguez-Tenreiro, R. 2001, *ApJ*, 550, 703
- Hodge, P. W. & Michie R. W. 1969, *AJ*, 74, 587
- Irwin, M. J., & Hatzidimitriou, D. 1995, *MNRAS*, 277, 1354
- Johnston, K. V., Sigurdsson, S., & Hernquist, L. 1999, *MNRAS*, 302, 771
- Kleyna, J. T., Geller, M. J., Kenyon, S. J., Kurtz, M. J., & Thorstensen 1998, *AJ*, 115, 2359
- Kroupa, P. 1997, *New Astron.*, 2, 139
- Martínez-Delgado, D., Alonso-García, J., Aparicio, A., & Gómez-Flechoso, M. A. 2001, *ApJ*, 549, L63
- Martínez-Delgado, D., Gómez-Flechoso, M. A., Aparicio, A., & Carrera 2002, *AJ*, submitted
- Mateo, M. 1998, *ARA&A*, 36,455
- Olszewski, E. W., & Aaronson, M. 1985, *AJ*, 90, 2221
- Odenkirchen, M., et al. 2001, *AJ*, 122, 2538
- Palma, C., Majewski, S. R., Siegel, M. H., Patterson, R. J., & Ostheimer, J. C. 2002, *AJ*, in press
- Schweitzer, A. E., Cudworth, K. M., & Majewski, S. R. 1997, in *ASP Conference Series*, vol. 127, *Proper Motions and Galactic Astronomy*, ed. R. M. Humphreys (San Francisco:ASP), 132

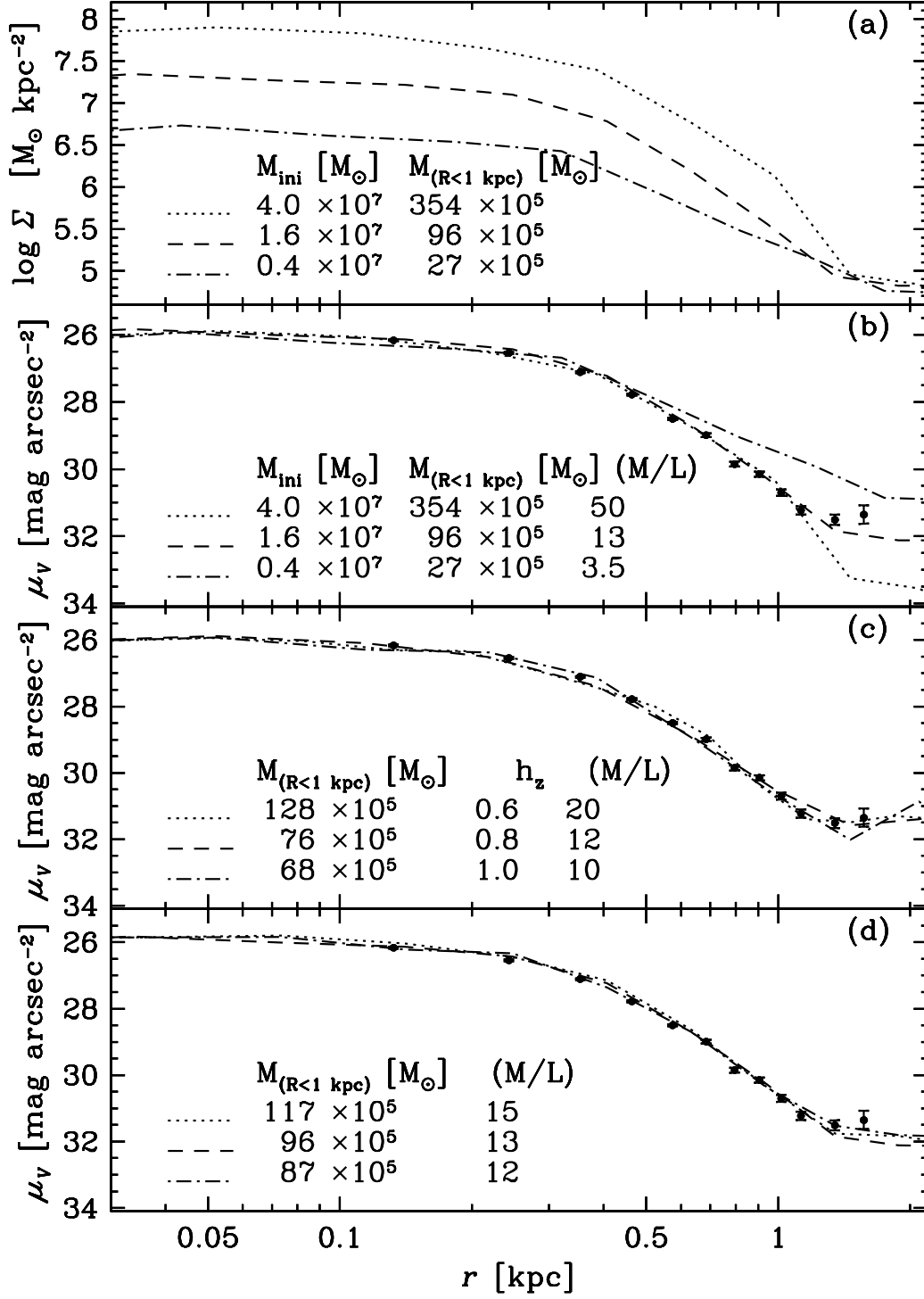


Fig. 1.— (a) Satellite surface density for three initial satellite masses. The three profiles have the same slope in the central region. (b) Luminosity profiles for the three satellite models assuming an M/L ratio in order to obtain a central surface brightness of $26 \text{ mag arcsec}^{-2}$.

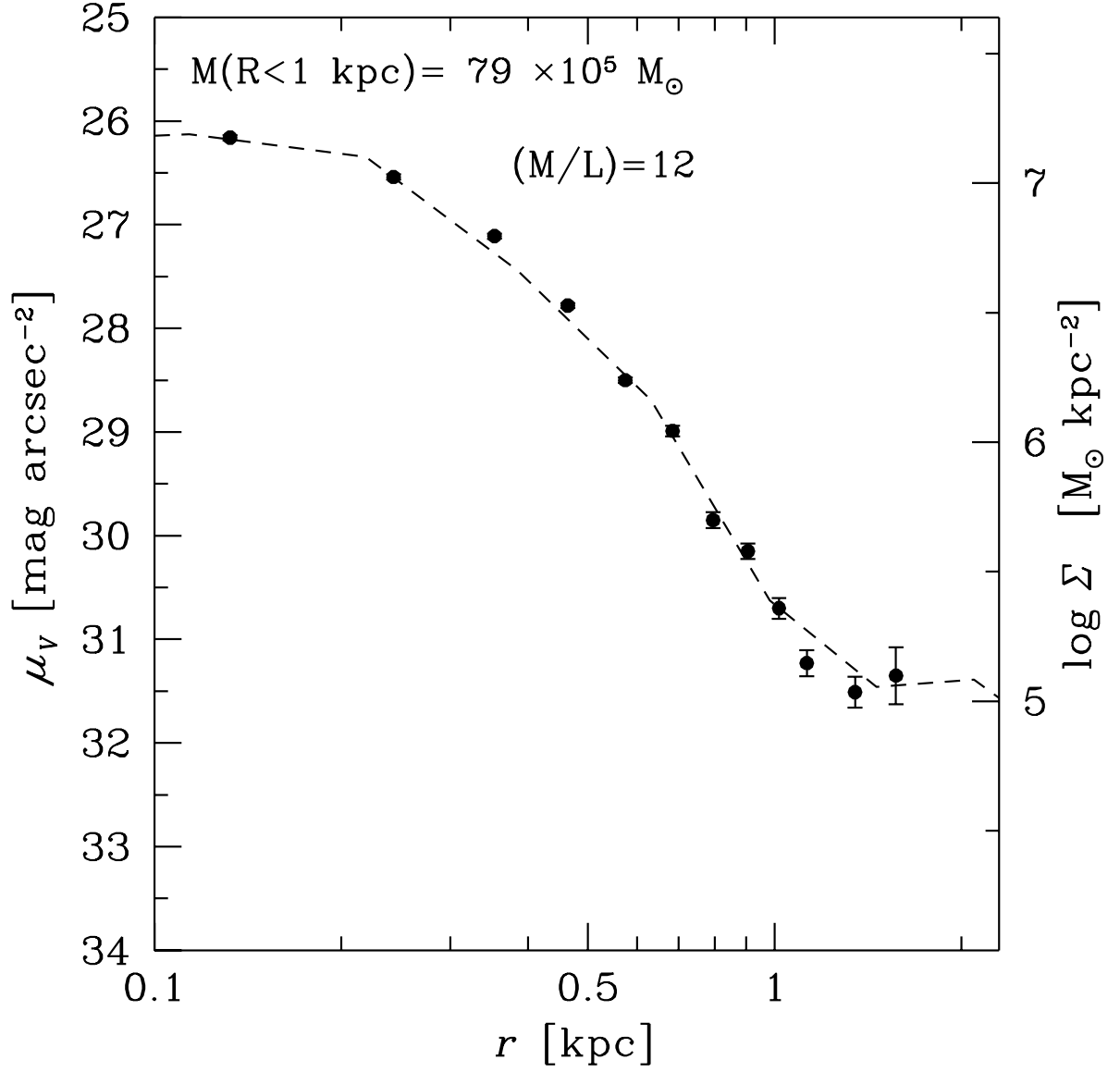


Fig. 2.— Surface brightness profile of the best UMi model (dash line), an $M/L = 12$ has been assumed. The observational data with the error bars are also plotted (dots).